Resource

Cell Reports

Molecular and Cellular Organization of Taste Neurons in Adult *Drosophila* Pharynx

Graphical Abstract

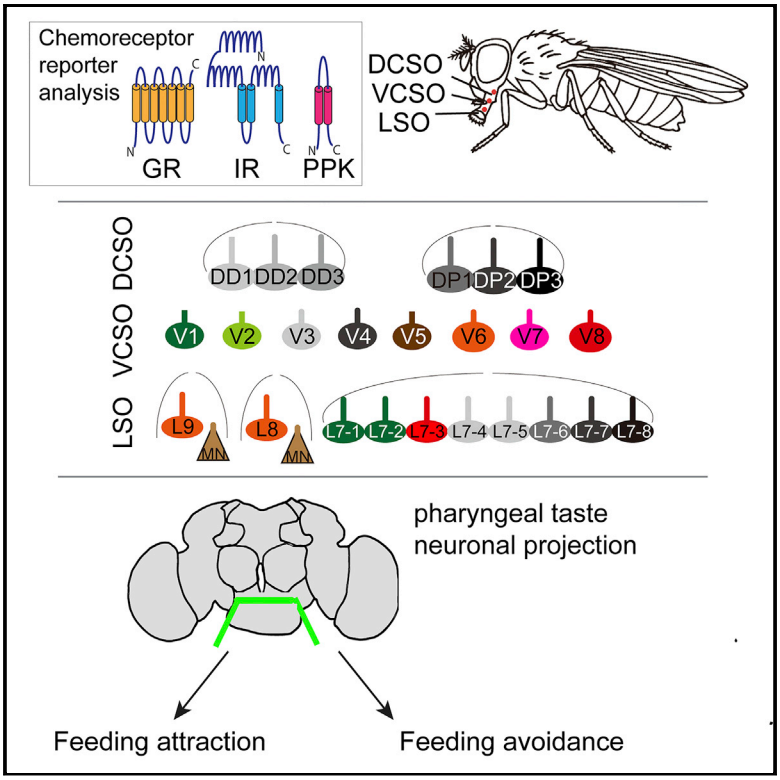

Authors

Yu-Chieh David Chen, Anupama Dahanukar

Correspondence

anupama.dahanukar@ucr.edu

In Brief

Chen and Dahanukar carry out a large-scale, systematic analysis to understand the molecular organization of pharyngeal taste neurons. Taking advantage of the molecular genetic toolkit that arises from this map, they use genetic dissection strategies to probe the functional roles of selected pharyngeal neurons in food choice.

Highlights

- Receptor-to-neuron maps of *Drosophila* adult pharyngeal taste organs
- Functional tests of molecularly predicted L-canavanine-sensing neurons
- Inducible activation survey of molecularly defined classes of internal taste neurons
- Identification of differences between external and internal taste neurons

Chen & Dahanukar, 2017, Cell Reports *21*, 2978–2991
December 5, 2017
https://doi.org/10.1016/j.celrep.2017.11.041

CellPress

OPEN ACCESS
CellPress

Cell Reports
Resource

Molecular and Cellular Organization of Taste Neurons in Adult *Drosophila* Pharynx

Yu-Chieh David Chen[1] and Anupama Dahanukar[1,2,3,*]
[1]Interdepartmental Neuroscience Program, University of California, Riverside, Riverside, CA 92521, USA
[2]Department of Molecular, Cell & Systems Biology, University of California, Riverside, Riverside, CA 92521, USA
[3]Lead Contact
*Correspondence: anupama.dahanukar@ucr.edu
https://doi.org/10.1016/j.celrep.2017.11.041

SUMMARY

The *Drosophila* pharyngeal taste organs are poorly characterized despite their location at important sites for monitoring food quality. Functional analysis of pharyngeal neurons has been hindered by the paucity of molecular tools to manipulate them, as well as their relative inaccessibility for neurophysiological investigations. Here, we generate receptor-to-neuron maps of all three pharyngeal taste organs by performing a comprehensive *chemoreceptor-GAL4/LexA* expression analysis. The organization of pharyngeal neurons reveals similarities and distinctions in receptor repertoires and neuronal groupings compared to external taste neurons. We validate the mapping results by pinpointing a single pharyngeal neuron required for feeding avoidance of L-canavanine. Inducible activation of pharyngeal taste neurons reveals functional differences between external and internal taste neurons and functional subdivision within pharyngeal sweet neurons. Our results provide roadmaps of pharyngeal taste organs in an insect model system for probing the role of these understudied neurons in controlling feeding behaviors.

INTRODUCTION

In *Drosophila*, taste neurons located in sensilla in several body regions sense and distinguish nutritive substances such as sugars, amino acids, and low salt, and potentially harmful ones such as high salt, acids, and a diverse variety of bitter compounds (Freeman and Dahanukar, 2015; Liman et al., 2014). Hair-like sensilla on the labellum, distal segments of the legs (tarsi), anterior wing margins, and ovipositor have access to chemicals in external substrates. Pit-like sensilla (taste pegs) on the oral surface have access only once the fly extends its proboscis and opens the labellar palps; similar sensilla in the pharynx have access only when food intake is initiated. Based on its anatomical position, the pharynx is considered to act as a gatekeeper to control ingestion, promoting the intake of appetitive foods and blocking that of toxins.

Three distinct internal taste organs are present in the adult fly pharynx: the labral sense organ (LSO), the ventral cibarial sense organ (VCSO), and dorsal cibarial sense organ (DCSO). The VCSO and DCSO are paired on opposite sides of the rostrum, whereas the LSO is located in the haustellum (Figures 1A and 1B). The organization and neuronal composition of all three organs, based on both light and electron microscopy data, have been described in detail (Gendre et al., 2004; Nayak and Singh, 1983; Stocker and Schorderet, 1981). Nine separate sensilla are present in the LSO, of which 1–6 are innervated by a single mechanosensory neuron each. The remaining three, named 7–9, are uniporous sensilla, a feature that ascribes chemosensory function to them. Sensillum 7 is the largest one, with eight chemosensory neurons. Sensilla 8 and 9 have two neurons each (one mechanosensory and one chemosensory). Although one study reported two sensilla in the VCSO (Nayak and Singh, 1983), we and two others (Stocker and Schorderet, 1981; Gendre et al., 2004) observed three sensilla in the VCSO, innervated by a total of eight chemosensory neurons. The DCSO has two sensilla, each containing three chemosensory neurons. Notwithstanding the availability of detailed anatomical descriptions of pharyngeal taste organs, little is known about their function. The internal location of these organs poses challenges for electrophysiological analysis of taste neurons located within them. Additionally, few molecular tools are currently described to manipulate the function of selected pharyngeal taste neurons.

The expression and function of members of several chemosensory receptor gene families such as gustatory receptors (Grs), ionotropic receptors (Irs), Pickpocket (Ppk) channels, and transient receptor potential channels (Trps) have been found in external gustatory receptor neurons (GRNs) of the labellum and the tarsal segments (Freeman and Dahanukar, 2015). A number of *Gr-* and *Ir-GAL4* drivers are also shown to label pharyngeal organs (Kwon et al., 2014; Koh et al., 2014), but only a few, including *Gr43a* and members of sweet *Gr* clade, *Gr2a*, *Ir60b*, and *TrpA1*, have been mapped to specific taste neurons (LeDue et al., 2015; Kang et al., 2010; Miyamoto et al., 2012; Kim et al., 2017; Joseph et al., 2017).

Here, we generate receptor-to-neuron maps for three pharyngeal taste organs by a systematic expression analysis of chemoreceptor reporter lines that represent Gr, Ir, and Ppk receptor families. The maps reveal a large and diverse chemoreceptor repertoire in the pharynx. Some receptors are expressed in combinations that are predictive of neuronal sweet or bitter taste function based on analysis of external GRNs. By contrast, some pharyngeal taste neurons express receptor combinations that are distinct from any that have been reported in other organs, leaving open questions about their functional roles. We

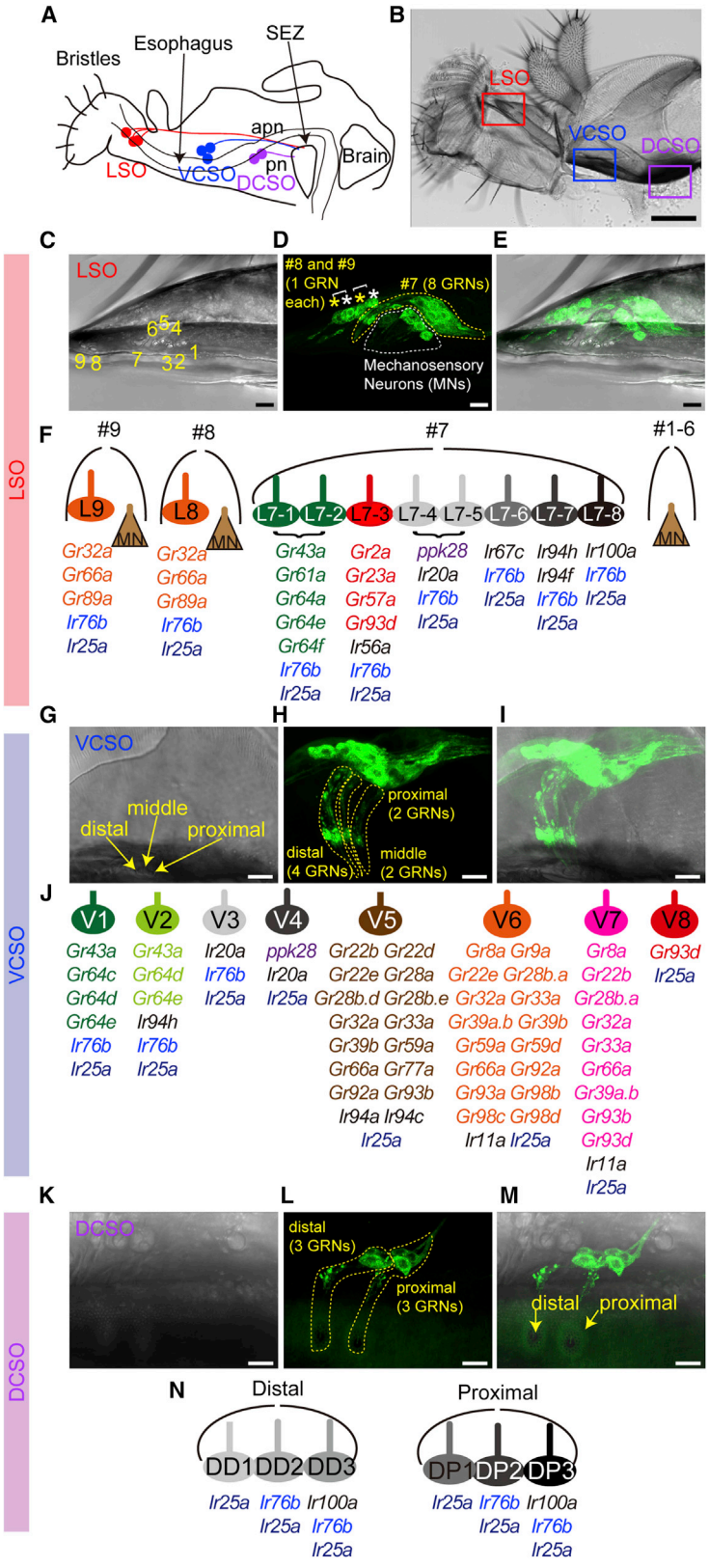

Figure 1. Receptor-to-Neuron Maps of Three Pharyngeal Taste Organs

(A and B) Schematic (A) and brightfield image of proboscis (B) showing three pharyngeal taste organs in wild-type flies. Taste neurons from the LSO and VCSO project to the subesophageal zone (SEZ) via the accessory pharyngeal nerve (apn); DCSO neurons project via the pharyngeal nerve (pn). Scale bar, 100 μm.

(C–E) *MJ94-GAL4* driven *UAS-mCD8-GFP*-labeled neurons in the LSO. Numbers in (C) indicate the nine LSO sensilla with a linear organization. In (D), the white dotted line and asterisks indicate mechanosensory neurons, and the yellow dotted line and asterisks indicate gustatory receptor neurons (GRNs). Brightfield (C) and fluorescence (D) images are merged (E) to map sensillar innervation. Scale bar, 10 μm.

(F) Schematic summary of a receptor-to-neuron map of the LSO as defined by reporter gene expression. MN, mechanosensory neuron.

(G–I) *Ir25a-GAL4* driven *UAS-mCD8-GFP* labeled neurons in the VCSO. In the brightfield image of the VCSO (G) yellow arrows mark three chemosensory sensilla with nonlinear organization, which precluded sensillar assignment of individual neurons in the following mapping analysis. In the fluorescence image (H), yellow dotted lines delineate groups of GFP labeled neurons in each sensillum, as derived from the merged brightfield/fluorescence image (I). Note that these representative images are the same as shown in Figure 3A. Scale bar, 10 μm.

(J) Schematic summary of a receptor-to-neuron map of the VCSO as defined by reporter gene expression.

(K–M) *MJ94-GAL4* driven *UAS-mCD8-GFP* labeled neurons in the DCSO. Brightfield (K) and fluorescence (L) images of the DCSO, merged (M) to visualize dendritic innervation of two DCSO chemosensory sensilla (yellow arrows). Yellow dotted lines (L) delineate groups of GFP labeled neurons in each sensillum. Scale bar, 10 μm.

(N) Schematic summary of a receptor-to-neuron map of the DCSO as defined by reporter gene expression.

validate the receptor-to-neuron maps derived from reporter gene expression by assessing roles of pharyngeal GRNs predicted to detect L-canavanine, a bitter tastant for which a complete receptor repertoire has been reported (Shim et al., 2015). Interestingly, a systematic activation analysis of different classes of pharyngeal taste neurons reveals functional differences between external and internal taste neurons for bitter avoidance and functional subdivision within pharyngeal sweet neurons for sweet acceptance. Together, our study provides a molecular map of pharyngeal taste organs, which will serve as a resource for future studies of the roles of pharyngeal taste neurons in food evaluation.

RESULTS

Chemoreceptor Reporter Expression in Pharyngeal Taste Organs

Although adult *Drosophila* pharyngeal taste organs have been anatomically characterized, little is known about receptor expression in sensory neurons housed within these organs. In a previous study, we described neurons in the LSO and VCSO that co-express multiple Grs belonging to the sweet clade (LeDue et al., 2015). However, sweet neurons account for a small fraction (4 of 24) of pharyngeal GRNs. We therefore systematically analyzed 43 *Gr-GAL4* drivers reported to label afferents in the pharyngeal nerve and termini in the subesophageal zone (SEZ) (Kwon et al., 2014). We mapped expression of 36 *Gr-GAL4* lines, which still showed strong expression in the pharynx (Table S1). We also examined a number of *Ir-GAL4* drivers, focusing on eight members of the *Ir20a* clade along with *Ir11a* and *Ir100a*, whose expression was reported in the pharynx (Koh et al., 2014, Croset et al., 2010). We included drivers for two broadly expressed Ir co-receptors, Ir25a and Ir76b, which are expressed in GRNs of external organs (Hussain et al., 2016, Zhang et al., 2013, Croset et al., 2010), and *ppk28-GAL4*, which marks water-sensing neurons in the labellum (Cameron et al., 2010). For most receptors, we tested two independent transgenic lines using *UAS-mCD8-GFP*. First, we identified the number of cells that were GFP positive in the pharynx. Next, we traced labeled dendrites to specific sensilla within each of the three pharyngeal taste organs. By using *MJ94-Gal4*, which labels most if not all chemosensory and mechanosensory neurons in the pharynx (Gendre et al., 2004), we were able to visualize one mechanosensory neuron each in LSO sensilla 1–6, eight GRNs in LSO sensillum 7, and one mechanosensory neuron and one GRN each in LSO sensilla 8 and 9 (Figures 1C–1F). In addition, we observed a total of eight GRNs in three VCSO taste sensilla (Figures 1G–1J) and a total of six GRNs in two DCSO taste sensilla (Figures 1K–1N) using *Ir25a-GAL4* and *MJ94-GAL4*, respectively. The three taste sensilla in the LSO, named 7, 8, and 9, are easily distinguishable from each other, as are the two proximal and distal sensilla in the DCSO. We were therefore able to map expression of each driver to one or more identified neurons within each sensillum of the LSO and DCSO (Figures 1F and 1N). The cuticular pores of the three sensilla in the VCSO, however, are clustered together in a nonlinear manner that precluded unambiguous mapping of labeled dendrites to their particular locations (Figure 1G). Thus, we mapped expression to specific neurons of the VCSO but did not attest sensillar assignments (Figure 1J). We introduced a nomenclature for pharyngeal GRNs, abbreviating location and assigning numbers as follows: L7-1 through L7-8 in LSO sensillum 7, L8 and L9 in LSO sensilla 8 and 9, V1–V8 in the VCSO, DD1–DD3 in the distal sensillum of the DCSO, and DP1–DP3 in the proximal sensillum of the DCSO.

In general, we found a total of 12 *Gr-GAL4* lines expressed in the LSO (Figure 2), including the 5 sweet *Gr-GAL4* drivers that we reported previously (LeDue et al., 2015), and 28 in the VCSO (Figures 3A–3H). A vast majority of the drivers labeled 1–3 neurons in the VCSO; several showed expression in 1–2 neurons in the LSO. We found *Gr-GAL4* lines that were expressed in the LSO alone, in the VCSO alone, and in both. Interestingly, the DCSO appeared to exclude *Gr*-expressing neurons (Figures 3I–3K). *ppk28-GAL4* also labeled cells exclusively in the LSO and VCSO. By contrast, we found *Ir*-expressing neurons in all pharyngeal taste organs. *Ir25a-GAL4*, in particular, labeled all GRNs in the LSO, VCSO, and DCSO, whose expression was validated with an Ir25a antibody (Figures 2C, 3A, and 3I; Movies S1, S3, and S4). *Ir76b-GAL4* also showed broad expression (Figures 2D, 3B, and 3J). All other drivers were expressed in smaller subsets of neurons (Figures 2E, 3F, and 3J). To further identify GRNs that express each driver, we performed a series of double-driver and double-labeling analyses. For the double-driver analyses, we examined selected pairwise combinations of drivers and compared the number of GFP-positive neurons for two *GAL4* drivers with those observed for a single *GAL4* driver alone (Figures 2H–2J, 3D, 3G, and 3H). We also took advantage of several *LexA* drivers to perform two-color analyses to confirm co-expression of drivers in the same neurons (Figures 2B, 2F, 2G, 3B, 3C, 3E, 3F, and 3K). Details of the mapping procedure are described in the following sections. Receptor-to-neuron maps generated from analyses of reporter lines are summarized in Figures 1F, 1J, and 1N.

Chemoreceptor Reporter Mapping in the LSO

In the LSO, we found that L8 and L9 expressed 3 *Gr-GAL4* lines (*Gr32a*, *Gr66a*, and *Gr89a*) (Figures 2A and 2B) representing commonly expressed receptors that are broadly expressed in external bitter taste neurons (Ling et al., 2014, Weiss et al., 2011). *Ir76b-* and *Ir25a-GAL4* labeled all taste neurons of sensilla 7–9 (Figure 2C and D; Movies S1 and S2). The expression of *Ir25a-GAL4* matched with the Ir25a antibody staining (Figure 2C). In sensillum 7 of the LSO, the L7-1 through L7-8 neurons could be grouped into six classes based on *GAL4* expression patterns (Figures 2E–2J). As previously described, two neurons, L7-1 and L7-2, expressed *Gr43a* along with other members of the sweet *Gr* clade (LeDue et al., 2015). Double labeling experiments with *Gr43a-LexA* and selected *GAL4* drivers that labeled 1–2 neurons of sensillum 7 revealed that cells expressing *Gr93d*/*Ir56a* (L7-3), *ppk28*/*Ir20a* (L7-4 and L7-5), *Ir67c* (L7-6), *Ir94f*/*Ir94h* (L7-7), and *Ir100a* (L7-8) were distinct from those expressing *Gr43a* (Figure 2F). A similar series of experiments with *ppk28-LexA* showed overlap with *GAL4* lines of *Ir20a*, but not *Gr93d*, *Ir56a*, *Ir67c*, *Ir94f*, *Ir94h*, and *Ir100a* (Figure 2G). Mapping of *Gr93d*, *Ir67c*, *Ir94f*, and *Ir100a GAL4* lines to separate neurons was confirmed by examining pairwise combinations of the four drivers; in all cases, animals with

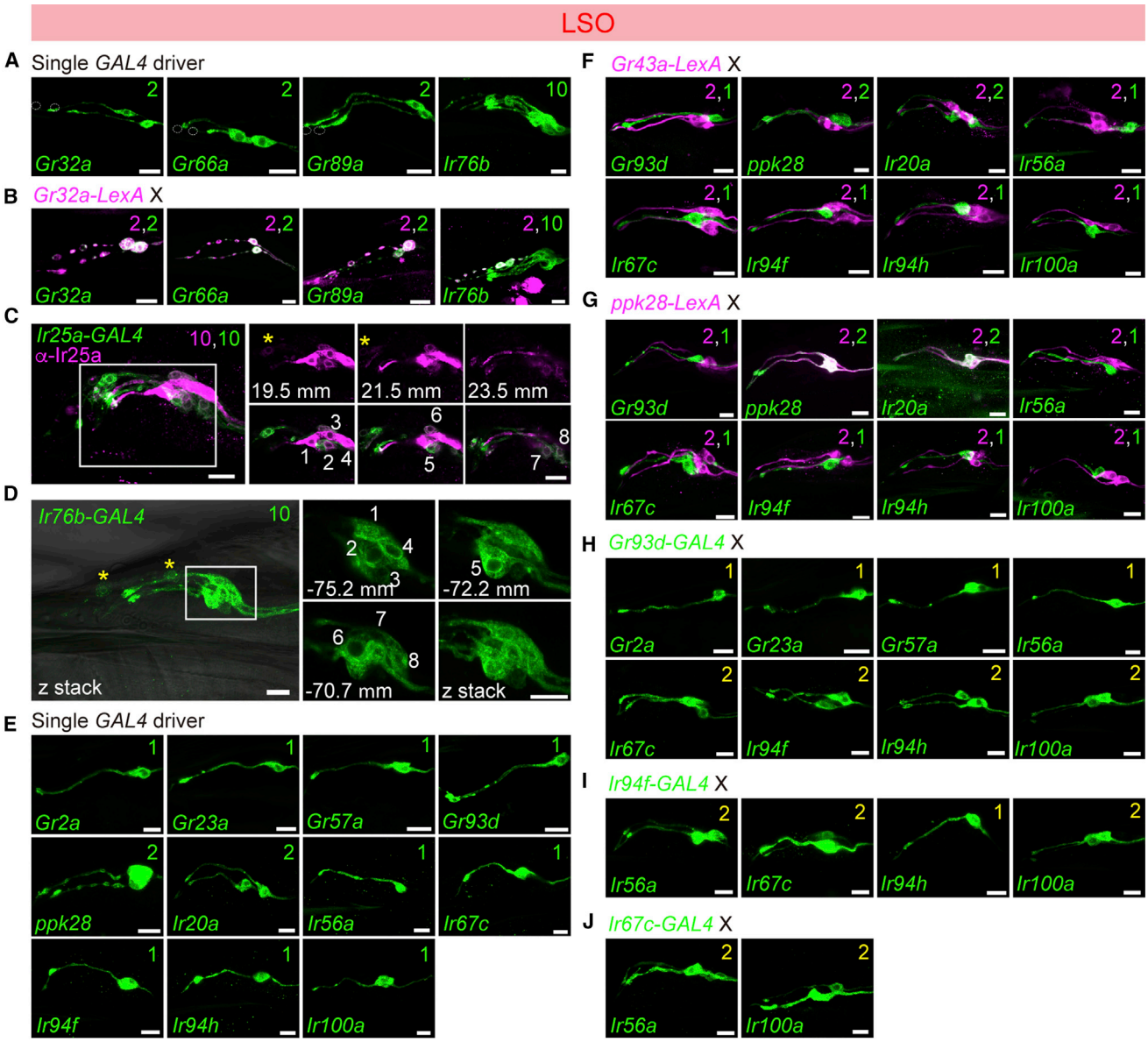

Figure 2. *Chemoreceptor-GAL4/LexA* Reporter Mapping in the Labral Sense Organ

(A–J) Expression of *Gr-GAL4* and *Ir-GAL4* lines in the LSO, tested with *UAS-mCD8-GFP* alone (green) (A, D, and E); co-stained with anti-Ir25a antibody (magenta) (C); tested in combination with *LexAop2-mCherry-HA* (magenta) in co-labeling experiments with *Gr32a-LexA* (B), *Gr43a-LexA* (F), *ppk28-LexA* (G); and in double-driver experiments with indicated *GAL4* drivers (H–J).

Numbers in (C) and (D) are used to label different cells visualized in different optical planes; positions along the *z*-axis are indicated in μm for the extracted slices. See also Movies S1 and S2. Numbers in top right corners indicate total numbers of green and magenta cells labeled by corresponding *GAL4/LexA* drivers. Numbers in yellow in top right corners in (H)–(J) indicate total numbers of GFP^+ cells observed with double *GAL4* driver analysis. Scale bar, 10 μm.

All panels show compressed z stacks, with the exception of those labeled with micrometers in (C) and (D), which represent single optical slices.

two drivers showed two labeled neurons, whereas each driver alone labeled only a single neuron. Additional double-driver experiments with either *Gr93d-* or *Ir94f-GAL4* indicated co-expression of four other receptors (*Gr2a*, *Gr23a*, *Gr57a*, and *Ir56a*) in the L7-3 neuron and *Ir94h* in the L7-7 neuron (Figures 2H–2J). We mapped *Ir100a* expression, along with *Ir25a* and *Ir76b*, in the L7-8 neuron, because *Ir100a* showed no co-expression with driver lines for *Gr43a*, *Gr93d*, *ppk28*, *Ir67c*, and *Ir94f*. A receptor-to-neuron map for the LSO generated from these results is shown in Figure 1F.

Chemoreceptor Reporter Mapping in the VCSO

In the VCSO, we found *Ir25a-GAL4* to be expressed in all eight neurons, as confirmed by an Ir25a antibody (Figure 3A; Movie S3). By contrast, *Ir76b* was expressed in only three of the eight GRNs. Two $Ir76b^+$ neurons were identified as V1 and

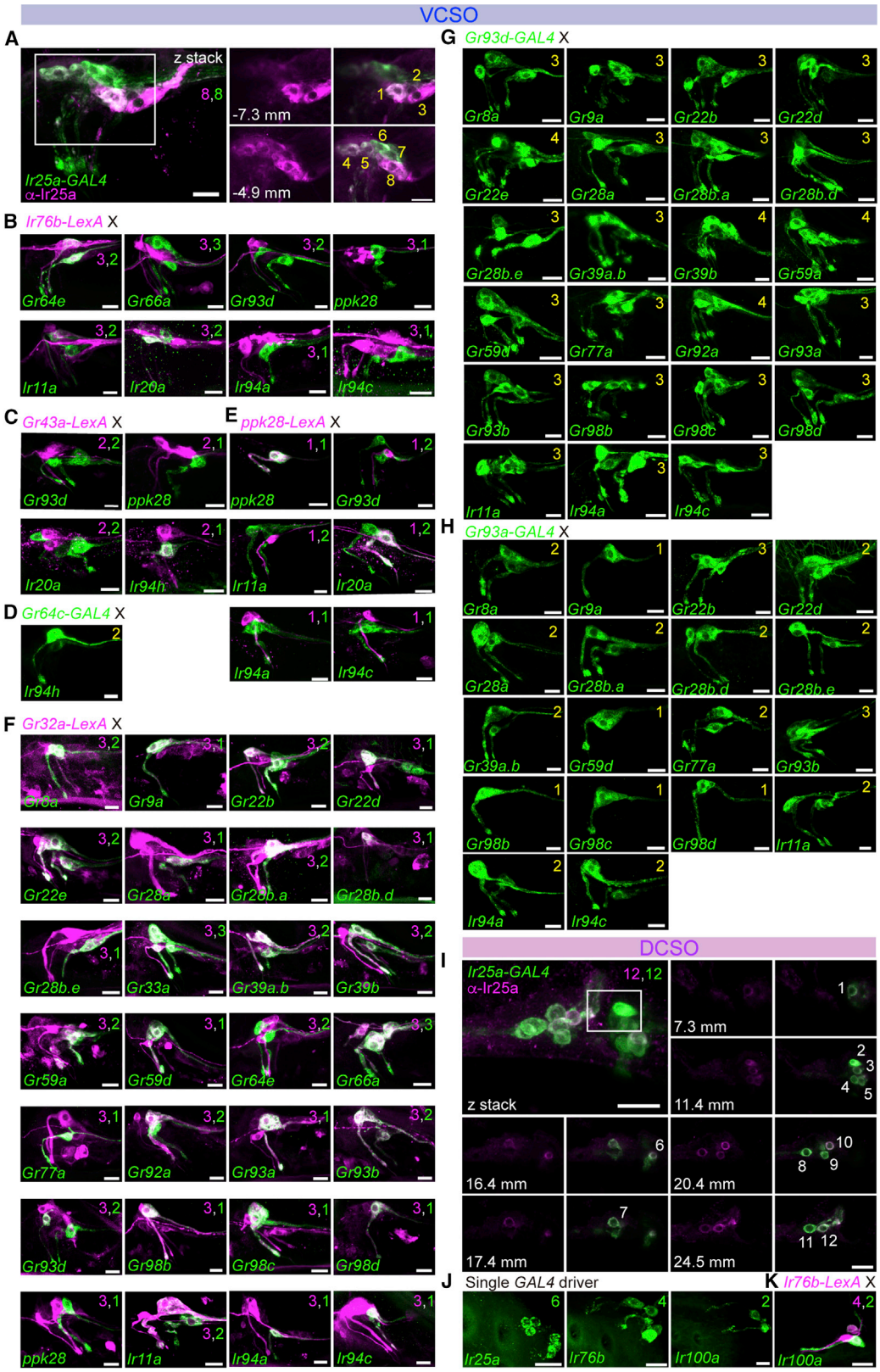

(legend on next page)

V2 due to co-expression with *Gr64e-GAL4*. The third *Ir76b*$^+$ neuron was identified as V3; it showed partial overlap with *Ir20a*, but not *ppk28* (V4), *Gr66a* (V5–V7), *Gr93d* (V7 and V8), *Ir11a*, *Ir94a*, or *Ir94c* (Figure 3B). Consistent with our previous observations with *Gr43a-GAL4* (LeDue et al., 2015), we found that two neurons, V1 and V2, expressed *Gr43a-LexA*. Double-labeling experiments with *Gr43a-LexA* showed overlap with *Ir94h-GAL4*, but not with *GAL4* lines for *Gr93d*, *ppk28*, or *Ir20a* (Figure 3C). Subsequently, we found that *Ir94h-GAL4* and *Gr64c-GAL4* independently marked each of the two *Gr43a*$^+$ neurons, identifying them as *Gr64c*$^+$ (V1) and *Ir94h*$^+$ (V2) (Figure 3D). We mapped *ppk28* expression to V4, because it was positive for one *Ir20a-GAL4* neuron, but not another (V3), and it did not overlap with drivers for *Gr43a*, *Ir76b*, *Gr32a*, and *Gr93d* (Figures 3B, 3C, 3E, and 3F).

One of the two cells labeled by *Gr93d-GAL4* overlapped with *Gr32a-LexA*, which was expressed in three cells (Figure 3F). Thus, *Gr32a* and *Gr93d* together accounted for four additional neurons: V5 (*Gr32a*$^+$), V6 (*Gr32a*$^+$), V7 (*Gr32a*$^+$, *Gr93d*$^+$), and V8 (*Gr32a*$^-$, *Gr93d*$^+$). We next systematically inspected overlap of *Gr32a-LexA* expression with *GAL4* drivers (Figure 3F). The three *Gr32a*$^+$ neurons also expressed *Gr33a* and *Gr66a*. The molecular identity of the three *Gr32a*$^+$ neurons could be further categorized by *Gr93a-* and *Gr93d-GAL4* (Table S2). 11 additional *Gr-GAL4* were mapped to V5 by virtue of overlap with *Gr32a-LexA* but exclusion from *Gr93a-* and *Gr93d-GAL4* cells. A single *Gr93a*$^+$ neuron was identified as V6, because *Gr93a-GAL4* expression overlapped with *Gr32a-LexA* but not with *Gr93d-GAL4*. Analysis of driver combinations with *Gr93a-* and *Gr93d-GAL4* mapped a group of 12 additional *Gr-GAL4* to V6 (Figures 3F–3H). The third *Gr32a*$^+$ neuron, identified as V7, was characterized as *Gr93a*$^-$, *Gr93d*$^+$. Double-driver analyses with *Gr93a-* and *Gr93d-GAL4* placed five additional *Gr-GAL4* in V7 (Figures 3F–3H). V8 was marked solely by expression of *Gr93d*, and no other *Gr-GAL4* drivers were co-expressed in this neuron. This series of experiments resolved mapping of all *Gr-GAL4* drivers expressed in the VCSO. We next turned to *Ir-GAL4* drivers. Both *Ir94a-* and *Ir94c-GAL4* were mapped to V5 because of co-expression with *Gr32a-LexA*, but not *Gr93d-* and *Gr93a-GAL4*, and confirmed by double-driver analysis that showed three GFP$^+$ neurons in animals that carried *Gr93d-GAL4* with either *Ir94a-* or *Ir94c-GAL4* (Figure 3G) and two GFP$^+$ neurons in animals that carried *Gr93a-GAL4* with either *Ir94a-* or *Ir94c-GAL4* (Figure 3H). *Ir11a-GAL4* was mapped to V6 and V7, because it overlapped with *Gr32a-LexA*, *Gr93a-GAL4*, and partially overlapped with *Gr93d-GAL4* (Figures 3F–3H). A receptor-to-neuron map for the VCSO generated from these results is shown in Figure 1J.

Chemoreceptor Reporter Mapping in the DCSO

In the DCSO, we found *Ir25a-GAL4* expression in all six neurons in the proximal and distal sensilla (Figure 3I; Movie S4). In addition, *Ir76b-GAL4* marked two of the three neurons in each sensillum (Figure 3J). Notably, *Ir100a-GAL4* showed expression in one taste neuron in each DCSO sensillum, which overlapped with *Ir76b-LexA* (Figure 3K). *Gr-GAL4* expression appears to be excluded from the DCSO, although we inconsistently observed expression of drivers for *Gr22b* and *Gr93d* (Figure S1). A receptor-to-neuron map for the DCSO generated from these results is shown in Figure 1N.

A Pharyngeal Taste Representation Map in the SEZ

Previous studies have shown that axons of taste neurons in pharyngeal taste organs travel via the pharyngeal and accessory pharyngeal nerves and terminate in the dorsoanterior region of the primary taste center, the SEZ (LeDue et al., 2015, Kwon et al., 2014, Stocker and Schorderet, 1981). Our receptor-to-neuron maps gave us an opportunity to examine axonal termini of bilaterally symmetrical pairs of taste neurons utilizing drivers that label single, or a small subset of, identified neurons. We tested all *chemosensory receptor-GAL4* drivers that label every neuronal class identified by mapping analysis, including four main classes of *Gr/Ir*-expressing pharyngeal GRNs: (1) sweet pharyngeal GRNs labeled by *Gr61a-/Gr64d-/Gr64e-GAL4* (Figure 4A), (2) putative water pharyngeal GRNs labeled by *ppk28-GAL4* (Figure 4B), (3) putative bitter pharyngeal GRNs labeled by *Gr77a-/Gr9a-/Gr33a-/Gr93d-/Gr66a-GAL4* (Figure 4C), and (4) *Ir*-expressing pharyngeal GRNs labeled by *Ir67c-/Ir94f-/Ir11a-/Ir20a-/Ir100a-/Ir76b-/Ir25a-GAL4* lines (Figure 4D). Because most of these drivers also showed expression in external GRNs, we examined labeled projections both in wild-type and in a *pox-neuro* (*poxn*) mutant background, in which all external taste bristles are transformed into mechanosensory bristles (Awasaki and Kimura, 1997, Nottebohm et al., 1992). As expected, in *poxn* mutants *UAS-mCD8-GFP* driven by *chemosensory receptor-GAL4* drivers showed expression in internal GRNs and their corresponding axonal projections in the SEZ (Figures 4A–4D). As reported previously (LeDue et al., 2015), *poxn* mutants also retained labeling in a few taste pegs present on the oral

Figure 3. *Chemoreceptor-GAL4/LexA* Reporter Mapping in Ventral and Dorsal Cibarial Sense Organs

(A–H) GFP expression (green) driven by indicated *Gr-GAL4* and *Ir-GAL4* lines in the VCSO co-stained with anti-Ir25a antibody (magenta) (A); tested in combination with *LexAop2-mCherry-HA* (magenta) in co-labeling experiments with *Ir76b-LexA* (B), *Gr43a-LexA* (C), *ppk28-LexA* (E), and *Gr32a-LexA* (F); and in double-driver experiments with indicated *GAL4* drivers (D, G, and H).

Numbers in (A) are used to label different cells visualized in different optical planes; positions along the z axis are indicated in μm for the extracted slices. See also Movie S3. Numbers in top right corners indicate total numbers of green or magenta cells labeled with corresponding *GAL4/LexA* reporters. Numbers in yellow in the top right corners in (D), (G), and (H) indicate total numbers of GFP$^+$ cells observed with double *GAL4* driver analysis.

(I) GFP expression (green) driven by *Ir25a-GAL4* in the DCSO co-stained with anti-Ir25a antibody (magenta). Numbers in panels are used to label different cells visualized in different optical planes; positions along the z axis are indicated in micrometers for the extracted slices. See also Movie S4. Scale bar, 10 μm.

(J and K) GFP expression (green) driven by indicated *Ir-GAL4* lines in the DCSO (J) or tested in combination with *LexAop2-mCherry-HA* (magenta) in co-labeling experiments with *Ir76b-LexA* (K). Numbers in the top right corners indicate total numbers of green and magenta cells labeled by corresponding *GAL4/LexA* reporters. See also Figure S1.

All panels show compressed z stacks, with the exception of those labeled with micrometers in (A) and (I), which represent single optical slices. Scale bar, 10 μm.

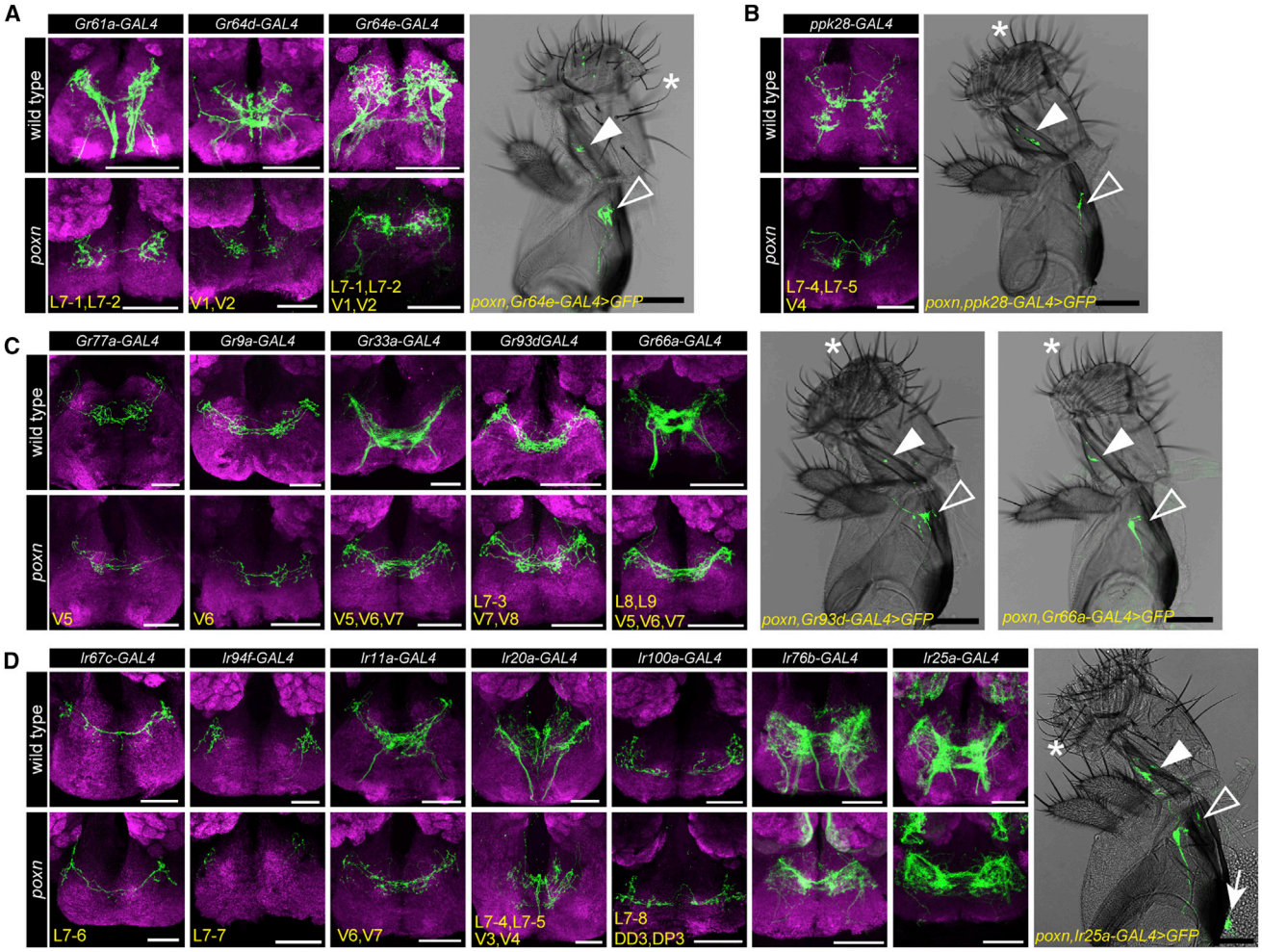

Figure 4. Axonal Projections of Different Classes of Pharyngeal GRNs in the Subesophageal Zone

(A–D) Images of the SEZ showing axonal termini (green) labeled by indicated *Gr-* or *Ir-GAL4* drivers in wild-type (w^{1118}, top) and *poxn* ($poxn^{\Delta M22\text{-}B5}/poxn^{70}$, bottom) flies. Four main classes of pharyngeal neuronal projections are presented: sweet pharyngeal GRNs (A), putative water pharyngeal GRNs (B), putative bitter pharyngeal GRNs (C), and *Ir*-expressing pharyngeal GRNs (D). Brightfield images of the proboscis show GFP cells (green) labeled by indicated *GAL4* driver in the LSO (closed arrowhead), VCSO (open arrowhead), and DCSO (arrow) in *poxn* mutants. Asterisks point to representative long, bent mechanosensory bristles, which are present in place of external taste hairs in *poxn* mutants. Scale bar, 100 μm. Neuropil is stained with anti-nc82 (magenta). Subsets of pharyngeal GRNs labeled by *GAL4* drivers named in bottom left corners. Also see Figures 1F, 1J, and 1N for nomenclature. Note the presence of a small subset of taste peg projections labeled by *Gr64e-/Ir76b-/Ir25a-GAL4* in the SEZ, and *Ir76b-/Ir25a-GAL4* labeled olfactory projections to antennal lobes in *poxn* mutants.

surface of the labellum; axons of these neurons terminate in characteristic, bilaterally symmetric S-shaped patterns in the SEZ. Axonal termini of pharyngeal GRNs were all found in the expected dorsoanterior region, with some differences in patterns of axonal arborization. We noticed that neurites of GRNs that are predicted to sense aversive tastants (e.g., *Gr77a-/Gr9a-/Gr33a-/Gr93d-/Gr66a-GAL4*) had extensive projections at the midline, whereas those predicted to sense appetitive tastants (e.g., *Gr61a-/Gr64d-/Gr64e-/ppk28-/Ir94f-GAL4*) were present in discrete regions on each ipsilateral side.

Pharyngeal Taste Projections Can Be Separated by Neurons and Organs

To characterize the projections of different classes of pharyngeal GRNs in the SEZ, we examined the overlap of *Gr43a*, *ppk28*, and *Gr93d* projections by testing combinations of *GAL4/LexA* drivers. We visualized single optical sections of fluorescence images, which revealed little overlap between *Gr43a*, *ppk28*, and *Gr93d*-labeled termini (Figure 5A), consistent with the idea that these GRNs, which are likely to sense different categories of tastants, have distinct representations in the SEZ. To examine whether GRNs of the same taste category originating in different pharyngeal taste organs target discrete areas of the SEZ, we compared axonal projections labeled by *Gr43a-LexA* (LSO and VCSO) and *Gr61a-GAL4* (LSO alone) in *poxn* mutants using two-color analysis. We note that *Gr43a-LexA* projections of olfactory neurons were also visualized via labial nerves in the antennal lobes of *poxn* mutants. We found *Gr43a-LexA* taste projections distributed in an anterior zone of the SEZ, labeling neurites in medial and lateral regions. Overlapping *Gr61a-GAL4* projections were found

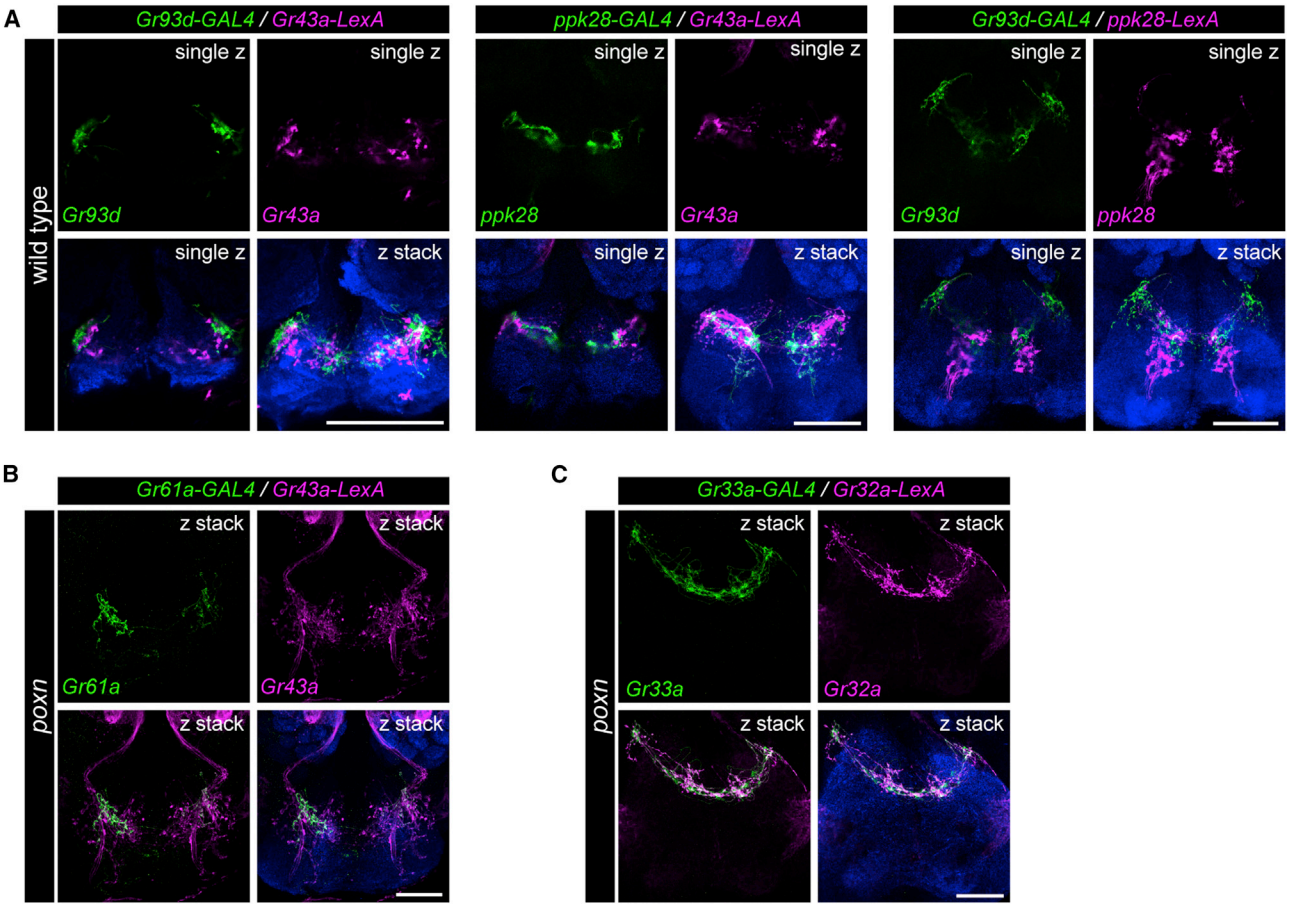

Figure 5. Pharyngeal Neurons of Different Categories or Locations Show Distinct Patterns of Axonal Projections in the Subesophageal Zone

(A) Axonal projections of pharyngeal GRNs labeled by different *GAL4/LexA* drivers in the SEZ in wild-type (w^{1118}) flies. Annotations in top right corners of each image indicate a single optical section (single z) to examine reporter co-localization, or compressed z stacks (z stack) for comparison. Neuropil is stained with anti-nc82 (blue). In all panels, scale bars represent 50 μm.

(B) Axonal projections labeled by *Gr61a-GAL4* (green) and *Gr43a-LexA* (magenta) in the SEZ in *poxn* ($poxn^{\Delta M22\text{-}B5}/poxn^{70}$) flies. Note the presence of intact olfactory projections to antennal lobes through labial nerves labeled by *Gr43a-LexA* in *poxn* mutants. Neuropil is stained with anti-nc82 (blue). Scale bar, 50 μm.

(C) Axonal projections labeled by *Gr33a-GAL4* (green) and *Gr32a-LexA* (magenta) in the SEZ in *poxn* ($poxn^{\Delta M22\text{-}B5}/poxn^{70}$) flies. Neuropil is stained with anti-nc82 (blue). Scale bar, 50 μm.

in the lateral areas but were limited or absent in the medial region, suggesting the pharyngeal sweet neuronal projections from the VCSO terminate medially as compared to those from the LSO (Figure 5B). The separation between putative bitter pharyngeal GRNs of the LSO and VCSO was less obvious when we compared *Gr32a-LexA* (LSO and VCSO) and *Gr33a-GAL4* (VCSO alone) labeling in *poxn* flies (Figure 5C), mainly due to extensive midline projections of these putative bitter pharyngeal GRNs. Overall, these results suggest that pharyngeal GRNs of different classes and/or different pharyngeal taste organs target distinct areas of the SEZ and may represent distinct neural circuits and possibly distinct functional roles.

Functional Validation of Pharyngeal Taste Receptor-to-Neuron Maps

We next wished to validate the results of our receptor-to-neuron maps, given the caveat that transgenic drivers, which we used to assess receptor expression patterns, may not always reflect endogenous expression patterns of receptors. In a previous study, we confirmed that *Gr64e-GAL4* does in fact label pharyngeal sweet GRNs using calcium imaging and behavior assays (LeDue et al., 2015). We therefore decided to focus on a different taste category to validate other neuronal identities. Specifically, we elected to test a bitter compound, L-canavanine, for two reasons. First, L-canavanine is known to activate bitter GRNs, but it does not inhibit sweet GRNs (French et al., 2015; Jeong et al., 2013), which can otherwise confound interpretations of feeding assays using sugar/bitter mixtures. Second, L-canavanine is the only bitter compound for which a complete receptor repertoire has been described (Shim et al., 2015). A recent study reported a high-affinity complex comprising Gr8a/Gr66a/Gr98b for detection of L-canavanine (Shim et al., 2015). Perusal of our receptor-to-neuron maps implicated a single *Gr66a* neuron, the V6 neuron in the VCSO, as a high-affinity sensor of L-canavanine.

We first silenced all *Gr66a* pharyngeal GRNs using the inwardly rectifying channel, Kir2.1, and tested behavioral

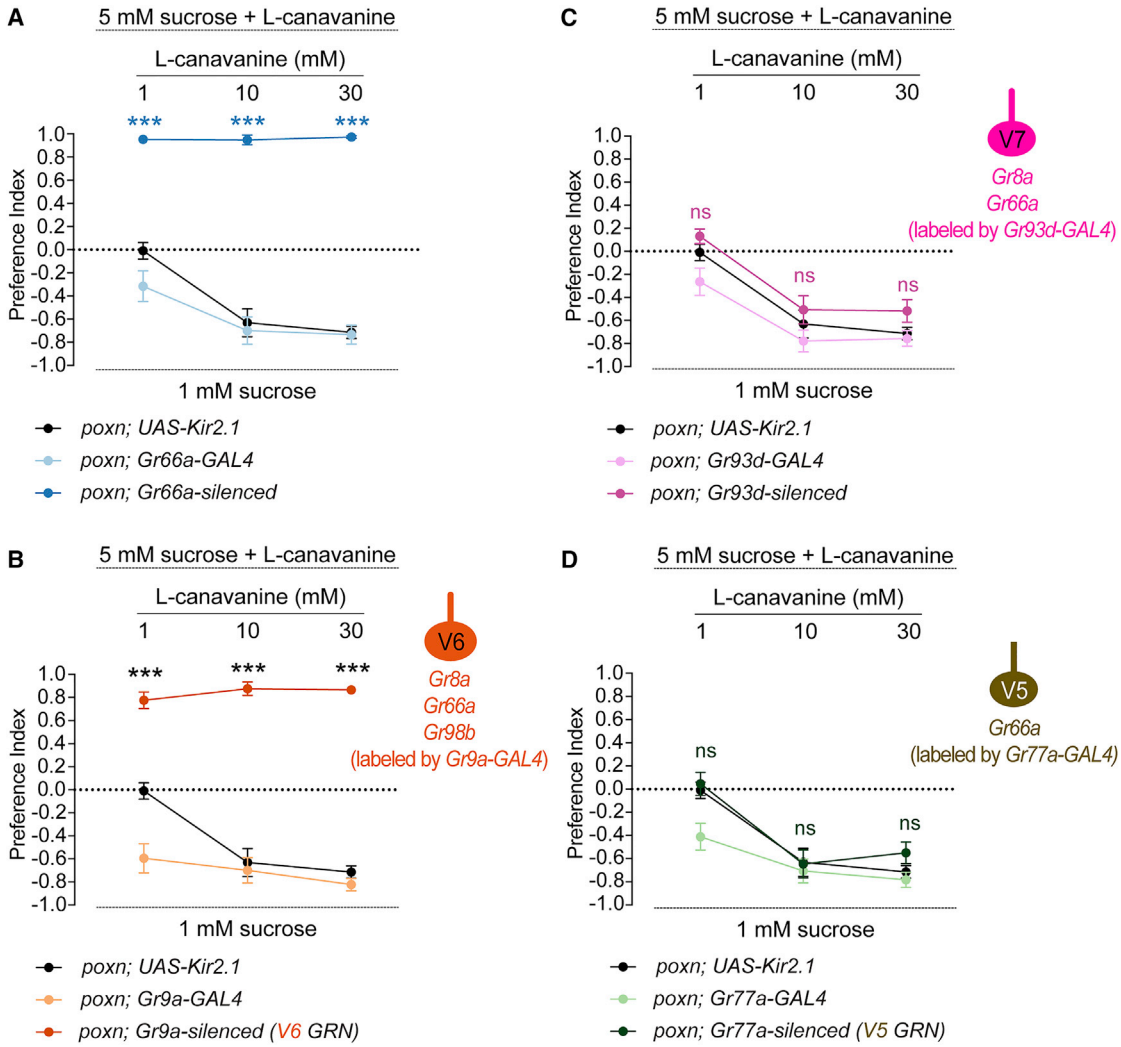

Figure 6. Genetic Silencing Experiments Support Receptor-to-Neuron Maps

(A–D) Mean preference index values from binary choice experiments with sucrose tested against a mixture of sucrose and L-canavanine at the indicated concentrations. All genetic manipulations with *Gr66a-GAL4* (A), *Gr9a-GAL4* (B), *Gr93d-GAL4* (C), and *Gr77a-GAL4* (D) were performed in a *poxn* mutant background ($poxn^{\Delta M22\text{-}B5}/poxn^{70}$). Schematics of identified VCSO neurons derived from Figure 3 indicating expression of *Gr8a-/Gr66a-/Gr98b-GAL4* are shown on the right of (B)–(D). n = 10–30. Error bars represent SEM. ***p < 0.0001 versus *UAS* control, two-way ANOVA with post hoc Tukey test (ns, not significant).

responses to various concentrations of L-canavanine mixed with 5 mM sucrose. Experiments were carried out in *poxn* mutants to exclude any contribution from external GRNs. As predicted, control flies showed avoidance of L-canavanine in a dose-dependent manner, which was completely abolished in *Gr66a*-silenced flies (Figure 6A). We then assessed the role of the V6 neuron in sensing L-canavanine using *Gr9a-GAL4*, which is expressed exclusively in this neuron. Notably, in the absence of a functional V6 neuron, flies lost the ability to avoid L-canavanine at all concentrations tested (Figure 6B), similar to *Gr66a*-silenced flies. This result provides functional evidence for L-canavanine receptor expression in the V6 neuron.

The previous study suggested that *Gr8a* and *Gr66a* together may be sufficient for a weak response to L-canavanine (Shim et al., 2015). We therefore tested the role of the *Gr8a/Gr66a*-labeled V7 neuron. Since a *GAL4* driver that is exclusively expressed in V7 is not available, we expressed Kir2.1 with *Gr93d-GAL4*, which would silence V7 along with two other neurons in the LSO (L7-3) and VCSO (V8). The resulting flies exhibited no difference in feeding avoidance of L-canavanine as compared to the *UAS* control at all concentrations of L-canavanine (Figure 6C). As an additional control, we silenced the V5 neuron specifically by *Gr77a-GAL4*, which does not express either *Gr8a* or *Gr98b* according to our reporter analysis. As predicted, this manipulation caused no reduction in L-canavanine avoidance (Figure 6D). We note that *Gr93d-* and *Gr77a*-silenced flies showed a significant difference in feeding avoidance of 1 mM L-canavanine as compared to the corresponding *GAL4* control, but not the *UAS* control, suggesting that the difference is likely due to the background effect of

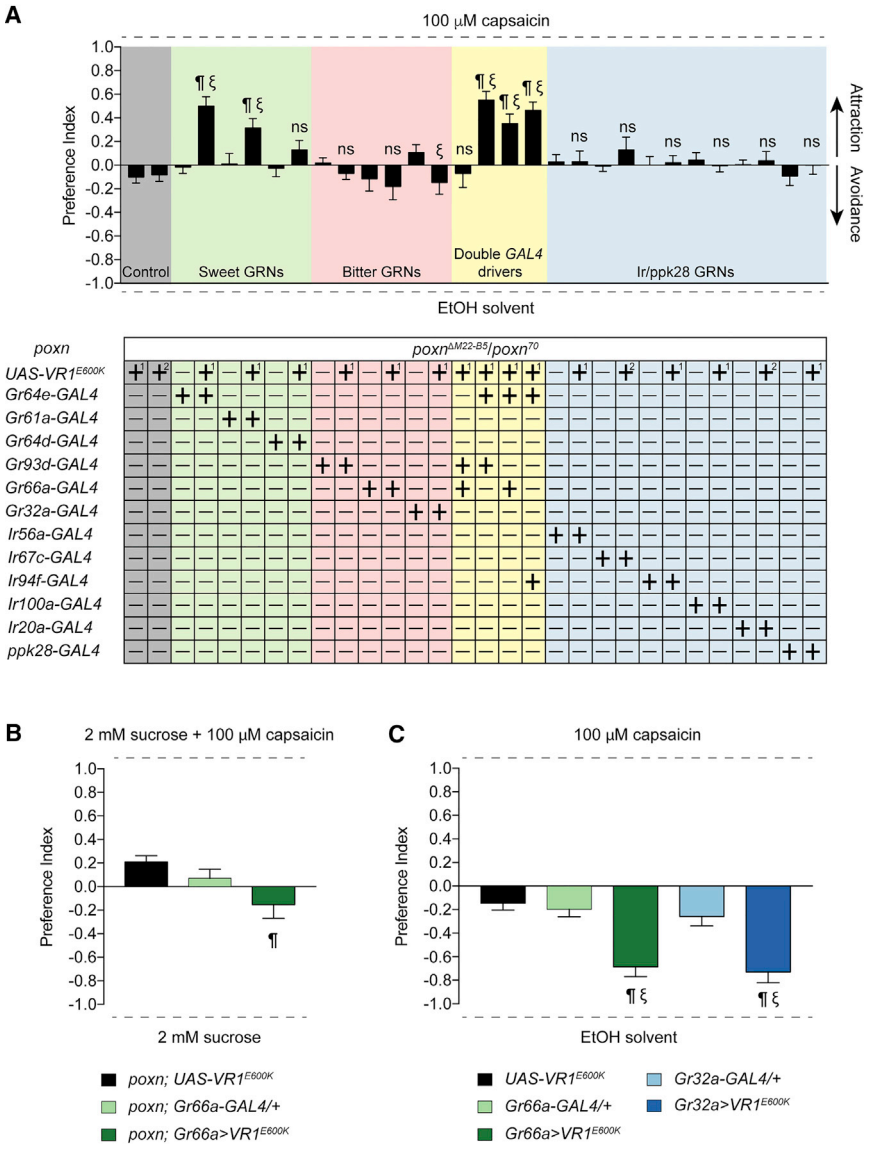

Figure 7. A Systematically Inducible Activation of Different Classes of Pharyngeal Neurons

(A) Mean preference index values from binary choice experiments with capsaicin tested against ethanol solvent. Genetic manipulations were performed in *poxn* mutant (*poxn*$^{\Delta M22\text{-}B5}$/*poxn*^{70}). Two different *UAS-VR1*^{E600K} controls are shown; [1] is a recombinant *of UAS-VR1*^{E600K} with the *poxn*$^{\Delta M22\text{-}B5}$ allele; [2] is a recombinant with the *poxn*^{70} allele. n = 19–30. Error bars indicate SEM; ¶ indicates significant difference from the corresponding *UAS* control, and ξ indicates significant difference from the corresponding *GAL4* control (for double-driver experiments, ξ indicates significant difference from both *GAL4* controls). $p < 0.05$, one-way ANOVA with Tukey test (ns, not significant).

(B) Mean preference index values from binary choice experiments with capsaicin-sucrose mixture tested against sucrose alone. Genetic manipulations were performed in *poxn* mutant (*poxn*$^{\Delta M22\text{-}B5}$/*poxn*^{70}). n = 28–32. Error bars indicate SEM; ¶ indicates significant difference from the corresponding *UAS* control. $p < 0.05$, one-way ANOVA with Tukey test.

(C) Results of binary-choice feeding assays performed using flies expressing *VR1*^{E600K} under the control of the indicated *GAL4* drivers in a wild-type background with only one *poxn*$^{\Delta M22\text{-}B5}$ allele. Tastants used were capsaicin and ethanol solvent. n = 10–20. Error bars represent SEM; ¶ indicates significant difference from the *UAS* control, and ξ indicates significant difference from the corresponding *GAL4* control. $p < 0.05$, one-way ANOVA with Tukey test (ns, not significant).

UAS-Kir2.1. Taken together, we identified V6 as a functional L-canavanine-sensing pharyngeal neuron, with V5 or V7 playing little if any role in sensing L-canavanine, on the basis of their molecular signatures.

Inducible Activation of Different Pharyngeal Taste Neurons Identifies Functional Differences between and within Different Taste Organs

We next wished to identify the valence that each class of pharyngeal taste neurons might carry in our feeding choice assay. The use of cognate tastants may not be ideal for such experiments for two main reasons. First, cross-modality interactions between tastants and GRNs (French et al., 2015; Jeong et al., 2013) confound interpretation of individual GRN valence. Second, a recent report has found sugar-sensing pharyngeal GRNs that have a negative effect on consumption (Joseph et al., 2017), suggesting that tastants defined as "appetitive" or "aversive" may not activate predictable sets of pharyngeal GRNs. Therefore, we expressed the mammalian capsaicin receptor (*UAS-VR1*^{E600K}) (Marella et al., 2006) under the control of selected *GAL4* drivers in *poxn* mutants and measured feeding preference for capsaicin (Figure 7A). Flies were tested in binary choice assays with 100 μM capsaicin and ethanol solvent as the two alternatives. All *GAL4* and *UAS* controls were tested, and none showed a preference for capsaicin. We found that *Gr64e* > *VR1*^{E600K} flies had a significant preference for capsaicin, demonstrating that activation of *Gr64e*$^{+}$ neurons in the LSO and VCSO is sufficient to trigger taste acceptance and ingestion. One caveat is that a few taste pegs would also be activated in *Gr64e* > *VR1*^{E600K} flies, and activation of taste pegs has been shown to be sufficient for feeding acceptance (Fischler et al., 2007). We next decided to activate *Gr64e*$^{+}$ neurons in the LSO alone (via *Gr61a-GAL4*) or in the VCSO alone (via *Gr64d-GAL4*). The former resulted in preference for capsaicin whereas the latter did not, suggesting some functional subdivision of pharyngeal sweet GRNs in driving feeding attraction to sugars.

Surprisingly, we did not observe significant feeding avoidance of capsaicin with the activation of putative bitter taste neurons

using either the *Gr66a-* or *Gr93d-GAL4* drivers. To rule out the possibility that expression via *Gr66a-GAL4* is too weak to drive functional levels of the capsaicin receptor, we confirmed these results using the *Gr32a-GAL4* driver, whose expression overlaps precisely with that of *Gr66a-GAL4*. The activation of *Gr32a* neurons also did not elicit significant capsaicin avoidance (Figure 7A). Neither did the combined activation of $Gr66a^{+}$ and $Gr93d^{+}$ neurons. A 10-fold greater concentration of capsaicin (1 mM) did not yield conclusive results, because it affected gelling of the agarose droplets and thwarted participation of adequate numbers of flies. We next tested whether an avoidance function for these neurons could be uncovered when the flies were induced to consume capsaicin. We found that *poxn* flies in which $Gr66a^{+}$ neurons were activated simultaneously with $Gr64e^{+}$ showed a non-significant reduction of mean PI for capsaicin compared to activation of $Gr64e^{+}$ alone (two-tailed t test, $p = 0.2931$, ns). A similar effect was not observed using *Gr64e-GAL4* combined with either *Gr93d* or *Ir94f* drivers. Thus, although not statistically significant, the reduction in mean PI was specifically observed with the *Gr66a* driver. We therefore tested whether activation of *Gr66a* neurons by capsaicin could induce feeding avoidance of a sugar/capsaicin mixture. This experimental paradigm uncovered activation of weak avoidance in *Gr66a* > $VR1^{E600K}$ flies as compared to the *UAS* control (one-way ANOVA with Tukey test, $p = 0.0079$) but not the corresponding *GAL4* control (one-way ANOVA with Tukey test, $p = 0.1012$ [not significant (ns)]) (Figure 7B). Thus, it appears that $VR1^{E600K}$-mediated activation of bitter GRNs does not elicit a strong feeding avoidance response. Although we cannot rule out the possibility that $VR1^{E600K}$ expression or function is weaker in bitter neurons, capsaicin-induced activation of external bitter neurons in wild-type flies using *Gr66a-* or *Gr32a-GAL4* caused strong feeding avoidance (Figure 7C). The two different outcomes may arise from functional differences between internal and external bitter taste circuits or from numerical differences in activation of bitter neurons.

No discernible phenotypes were observed upon activation or neurons of unknown function marked by *Ir56a*, *Ir67c*, *Ir94f*, *Ir100a*, or *Ir20a* or of neurons expressing the Ppk28 water receptor. It is possible that these pharyngeal taste neurons may be involved in other behaviors, such as choice of oviposition substrate, as has been reported for *Gr66a* (Joseph and Heberlein, 2012). Alternatively, their roles in feeding behaviors may be dependent on the context, such as prior experience, internal state, or complexity of food substrate.

DISCUSSION

Internal pharyngeal taste organs are the least explored taste organs, despite their obvious importance in insect feeding behaviors, which are crucial drivers for damaging crops and vectoring disease. Here, we investigate the organization of pharyngeal taste neurons by generating maps of *chemoreceptor-GAL4* expression, which showcase the complex molecular signatures and groupings of these in the pharynx.

The receptor-to-neuron maps of pharyngeal taste organs suggest a high degree of molecular complexity, with co-expression of different chemoreceptor family members in many pharyngeal GRNs. In particular, none of the pharyngeal GRNs were found to express *Gr* genes alone; rather, one or more *Ir* genes were always expressed in the same neurons. *Gr* and *Ir* genes are also co-expressed in some external sweet and bitter-sensing GRNs (van Giesen et al., 2016; Croset et al., 2010). Thus, both classes of receptors are likely to contribute to responses of *Gr*/*Ir*-expressing neurons in the LSO and VCSO, but whether they interact functionally or act independently remains to be determined. In the LSO, expression of sweet *Grs* and *Ir76b* overlaps in pharyngeal sweet GRNs, as observed in tarsi as well (Ganguly et al., 2017). In the pharynx, we also found co-expression of *ppk28* with *Ir* genes, which has not been described for external GRNs. These observations invite explorations of possible crosstalk, and its functional significance, between the two classes of receptors.

Pharyngeal GRNs also exhibit distinctive functional groupings. All external bitter GRNs have always been found grouped with sweet GRNs in taste hairs. By contrast, canonical sweet and bitter GRNs appear to segregate in different sensilla in the LSO, which is most well characterized for this perspective. L8 and L9 may be functionally identical and house only one *Gr66a*-expressing bitter GRN each, whereas L7 contains two sweet GRNs (L7-1 and L7-2). Moreover, external hairs typically have two to four GRNs, each of which has a distinct functional profile. In the LSO we find duplications (L7-1 and L7-2 are identical, as are L7-4 and L7-5), although differences between these pairs of GRNs may emerge as additional chemoreceptors are mapped in the pharynx. Finally, it is difficult to ascribe putative functions to most pharyngeal GRNs based on existing knowledge of receptor function in external counterparts. The L7-3 *Gr*-expressing neuron, for example, does not express members of the sweet clade, but neither does it express any of the common bitter Grs (*Gr32a*, *Gr66a*, and *Gr89a*) that would corroborate its role as a bitter GRN. Similarly, with the exception of salt neurons that may express *Ir76b* alone, there are few known functions for GRNs that solely express *Ir* genes. One possibility is that some of these GRNs possess novel chemoreceptor family ligand interactions. For example, L7-7 is involved in sensing sucrose but limiting sugar ingestion, representing an *Ir* neuron that operates in a negative circuit module for sugar intake (Joseph et al., 2017). In addition, another recent study suggests that TRPA1 expression in L8 and L9 of the LSO is involved in feeding avoidance to bacterial endotoxins lipopolysaccharides (LPS) (Soldano et al., 2016). Alternatively, some pharyngeal GRNs may evaluate characteristics other than palatability, such as temperature or viscosity. *Ir25a*, which is broadly expressed in all 24 pharyngeal GRNs, is required for cool sensing and thermosensing (Ni et al., 2016; Chen et al., 2015). It will be worth investigating whether one or more pharyngeal GRNs act to integrate information about temperature and chemical quality of food substrates.

Expression analyses also hint at some functional subdivisions between pharyngeal taste organs. The LSO contains a smaller proportion of *Gr*-expressing neurons than the VCSO, which also expresses a larger number of *Gr* genes that are co-expressed with *Gr66a*. Thus, we might expect broader bitter taste function in the VCSO. By contrast, sweet taste function appears to be more dominant in the LSO; its sweet GRNs express more

sweet *Gr-GAL4* drivers than the ones in the VCSO, and their activation is sufficient to drive feeding preference. VCSO sweet GRNs fail to promote ingestion by themselves but may contribute to an increase in feeding preference when activated simultaneously with those in the LSO. Thus, there may be synergistic or hierarchical interactions between LSO and VCSO sweet taste circuits, with the latter coming into play only once the former is activated. The finding that *Gr* and *Ir* genes are expressed in the LSO and VCSO but only *Ir* genes in the DCSO is also striking and raises the possibility that the DCSO, which is present at the most internal location relative to the others, may serve a unique role in controlling ingestion.

Based on its molecular signature, we identify the V5 neuron as an L-canavanine-sensing neuron in the pharynx. As predicted, feeding avoidance of L-canavanine is dependent on V5. It was thus unexpected that capsaicin-mediated activation of bitter pharyngeal GRNs, which include V5, did not induce strong feeding avoidance either in the absence or presence of sugar. Because the strength and pattern of pharyngeal neuronal activation by bitter tastants or capsaicin is unknown, it is possible that capsaicin response may be weaker than that of canonical bitter tastants. Alternatively, sweet and bitter inputs from internal and external neurons may be summed differently. It is known that activation of one or few external sweet neurons can lead to proboscis extension (Dethier, 1976; Keene and Masek, 2012), for example, but a larger number of bitter neurons may need to be activated for avoidance.

The afferents of pharyngeal GRNs target regions of the SEZ that are distinct from areas in which afferents from labellar and tarsal GRNs terminate (Kwon et al., 2014). Interestingly, pharyngeal GRN projections between molecularly different classes of neurons, as well as between GRNs of the LSO and VCSO, are also distinct. Projections of sugar-sensing GRNs were found in separate ipsilateral regions, whereas those of neurons predicted to detect aversive tastants were found at the midline, suggesting the presence of contralateral termini. These observations may inform future functional studies of pharyngeal GRNs. L7-6 neurons, for example, would be predicted to sense aversive compounds based on the presence of their termini at the midline. Analysis of pharyngeal GRN projections also suggests distinct connectivity to higher order neuronal circuits (Yapici et al., 2016). With the molecular tools described here, future investigations of pharyngeal GRNs and pharyngeal taste circuits will provide insight into how internal taste is integrated with external taste to control various aspects of feeding behavior.

EXPERIMENTAL PROCEDURES

Fly Strains

Flies were reared on standard cornmeal-dextrose-agar food at 25°C and 60%–70% relative humidity under a 12 hr/12 hr dark/light cycle. The following fly lines were used: *MJ94-GAL4* (a gift from L. Griffith, Brandeis University) *Gr-GAL4* (Ling et al., 2014; Weiss et al., 2011), *Gr66a-GAL4* (Bloomington *Drosophila* Stock Center [BDSC] 28801), *Ir-GAL4* (Koh et al., 2014), *Ir11a-GAL4* (BDSC 41742), *Ir100a-GAL4* (BDSC 41743), *Ir76b-GAL4* (BDSC 41730), *Ir25a-GAL4* (BDSC 41728), *ppk28-GAL4* (Cameron et al., 2010), *Gr43a-LexA* (Miyamoto and Amrein, 2014), *Gr32a-LexA* (Fan et al., 2013), *Ir76b-LexA* (Ganguly et al., 2017), *ppk28-LexA* (Thistle et al., 2012), *UAS-Kir2.1* (Baines et al., 2001), *UAS-VR1^{E600K}* (Marella et al., 2006), *poxn$^{\Delta M22\text{-}B5}$* (Boll and Noll, 2002), *poxn^{70}* (Awasaki and Kimura, 1997), *UAS-mCD8-GFP* (Weiss et al., 2011), and *LexAop2-6XmCherry-HA* (BDSC 52271, 52272). For experiments using *poxn* mutants, we confirmed the *poxn* mutant background in all sorted flies by observing the transformed long and bent mechanosensory hairs in the labellum, as well as the fused three tarsal segments in the legs.

Immunohistochemistry

At least 50 flies per genotype were anesthetized on ice, and the proboscis and brain tissue were dissected in 1× PBST (PBS with 0.3% Triton X-100) and fixed for 30 min with 4% paraformaldehyde in 1× PBST at room temperature. After three washes with 1× PBST, samples were blocked with 5% normal goat serum (Sigma, G9023) in 1× PBST. Tissues were incubated in primary antibody solutions for 3 days at 4°C. Primary antibodies were chicken anti-GFP (1:5,000; Abcam, ab13970), rabbit anti-GFP (1:1,000; Invitrogen, A11122), rabbit anti-DsRed (1:200; Clontech Laboratories, #632496), rabbit anti-Ir25a (1:500; a gift from L. Vosshall, Rockefeller University), and mouse anti-nc82 (1:20; DSHB). Secondary antibodies (1:400; Invitrogen) were goat anti-chicken Alexa 488, goat anti-rabbit Alexa 488 and Alexa Fluor 546, and goat anti-mouse Alexa Fluor 568 and 647. Samples were mounted in 80% glycerol in 1× PBST or Vectashield antifade mounting medium (Vector Laboratories, H-1000) and stored at 4°C. Fluorescent images were acquired using a Leica SP5 confocal microscope with 400 Hz scan speed in 512 × 512 or 1,024 × 1,024 pixel formats. Image stacks were acquired at 1-μm optical sections. Unless otherwise noted, all images were presented as maximum projections of the z stack generated using Leica LAS AF software.

Expression Analyses

Expression patterns of *Gr/Ir/ppk-GAL4/LexA* lines were mapped in the three pharyngeal taste organs using *UAS-mCD8-GFP* and *LexAop2-6XmCherry-HA* reporters. For most chemosensory receptors, we tested two or more independent reporter lines. Initial analysis was performed through live fluorescence imaging with at least 50 flies per line. The number of pharyngeal GRNs labeled by independent driver lines was consistent, although different signal intensities were observed across individual lines for the same receptor. We selected one representative line with stronger live fluorescence signal for further immunofluorescence mapping and behavioral experiments. For double-driver analysis, the *UAS-mCD8-GFP* transgene was under the control of two different *Gr-GAL4* drivers and the number of GFP-labeled neurons was compared to flies containing a single *Gr-GAL4* driver alone. Images were acquired using a Leica SP5 confocal microscope.

Binary Choice Feeding Assays

Feeding preference assays were performed as described previously (Charlu et al., 2013). Sucrose (S7903) and L-canavanine (C1625) were obtained from Sigma-Aldrich and dissolved in water; capsaicin (M2028) was also obtained from Sigma-Aldrich and prepared in ethanol. Briefly, flies were sorted into groups of 10 males and 10 females upon eclosion and aged for 5–8 days. Because *poxn* mutant male flies are sterile, we added two heterozygous males with curly wings (*poxn/CyO*) in each group to ensure that all sorted females were mated. Heterozygous males were discarded during scoring for abdominal color. Flies were starved for 24 hr on water-saturated tissues and then placed in tight-fit Petri dishes (Falcon, catalog no. 35-1006) with eighteen 10 μL dots of 0.75% agarose that alternated in tastant and color using either 25 mg/mL indigo carmine (Sigma, I8130) or 50 mg/mL sulforhodamine B (Sigma, 230162). We swapped dyes for each tastant with similar numbers of trials to account for any dye preference. Flies were allowed to feed for 2 hr at 25°C in a dark, humidified chamber, after which they were frozen and scored for abdomen color by dissecting the guts within 24 hr. Trials with participation lower than 50% were excluded. Preference index (PI) was calculated as ((number of flies labeled with the tastant color) − (number of flies labeled with the control color)) / (total number of flies that fed). Thus, a PI of 0 would indicate equal preference between the two choices. In all cases, PI values were calculated for mixed populations of males and females.

Experimental Design and Statistical Analysis

All data are presented as mean ± SEM. Statistical tests were conducted using Prism 7 (GraphPad Software). All experiments were performed in parallel with

both control and experimental genotypes. Complete genotypes used in this study are listed in Table S3. Complete statistics evaluations with the exact number of trials for each group are listed in Table S4. The sample size for each experiment was based on previously published reports. All independent trials were performed over 2 days. To improve normality and homogeneity of variances, we arcsine-transformed the square root of preference indices prior to analysis. Differences between means of different groups were evaluated for statistical significance with parametric ANOVA followed by post hoc Tukey multiple comparisons test.

SUPPLEMENTAL INFORMATION

Supplemental Information includes one figure, four tables, and four movies and can be found with this article online at https://doi.org/10.1016/j.celrep.2017.11.041.

ACKNOWLEDGMENTS

This work was funded by grants from the Whitehall Foundation (2010-12-42), NIH (R01DC013587 and R01DC014092), and National Science Foundation (IOS-1149667). Y.-C.C. is a Howard Hughes Medical Institute International Student Research Fellow. We thank B. Jablonska for technical support and M. Blick, R. Joseph, M. Gordon, J. Carlson, and members of the Dahanukar lab for helpful comments on the manuscript. We are grateful to H. Amrein, J. Carlson, M. Gordon, L. Griffith, K. Scott, and N. Shah for sharing fly strains and L. Vosshall for the anti-Ir25a antibody. Stocks were also obtained from the Bloomington *Drosophila* Stock Center (NIH P40OD018537).

AUTHOR CONTRIBUTIONS

Conceptualization, Y.-C.C. and A.D.; Methodology, Y.-C.C. and A.D.; Investigation, Y.-C.C.; Validation, Y.-C.C.; Formal Analysis, Y.-C.C.; Writing – Original Draft, Y.-C.C., Writing – Review & Editing, Y.-C.C. and A.D.; Visualization, Y.-C.C.; Supervision, A.D.; Funding Acquisition, A.D.

DECLARATION OF INTERESTS

The authors declare no competing interests.

Received: September 5, 2017
Revised: October 18, 2017
Accepted: November 10, 2017
Published: December 5, 2017

REFERENCES

Awasaki, T., and Kimura, K. (1997). pox-neuro is required for development of chemosensory bristles in Drosophila. J. Neurobiol. *32*, 707–721.

Baines, R.A., Uhler, J.P., Thompson, A., Sweeney, S.T., and Bate, M. (2001). Altered electrical properties in Drosophila neurons developing without synaptic transmission. J. Neurosci. *21*, 1523–1531.

Boll, W., and Noll, M. (2002). The Drosophila Pox neuro gene: control of male courtship behavior and fertility as revealed by a complete dissection of all enhancers. Development *129*, 5667–5681.

Cameron, P., Hiroi, M., Ngai, J., and Scott, K. (2010). The molecular basis for water taste in Drosophila. Nature *465*, 91–95.

Charlu, S., Wisotsky, Z., Medina, A., and Dahanukar, A. (2013). Acid sensing by sweet and bitter taste neurons in Drosophila melanogaster. Nat. Commun. *4*, 2042.

Chen, C., Buhl, E., Xu, M., Croset, V., Rees, J.S., Lilley, K.S., Benton, R., Hodge, J.J., and Stanewsky, R. (2015). Drosophila ionotropic receptor 25a mediates circadian clock resetting by temperature. Nature *527*, 516–520.

Croset, V., Rytz, R., Cummins, S.F., Budd, A., Brawand, D., Kaessmann, H., Gibson, T.J., and Benton, R. (2010). Ancient protostome origin of chemosensory ionotropic glutamate receptors and the evolution of insect taste and olfaction. PLoS Genet. *6*, e1001064.

Dethier, V.G. (1976). The Hungry Fly: A Physiological Study of the Behavior Associated with Feeding (Harvard University Press).

Fan, P., Manoli, D.S., Ahmed, O.M., Chen, Y., Agarwal, N., Kwong, S., Cai, A.G., Neitz, J., Renslo, A., Baker, B.S., and Shah, N.M. (2013). Genetic and neural mechanisms that inhibit Drosophila from mating with other species. Cell *154*, 89–102.

Fischler, W., Kong, P., Marella, S., and Scott, K. (2007). The detection of carbonation by the Drosophila gustatory system. Nature *448*, 1054–1057.

Freeman, E.G., and Dahanukar, A. (2015). Molecular neurobiology of Drosophila taste. Curr. Opin. Neurobiol. *34*, 140–148.

French, A.S., Sellier, M.J., Ali Agha, M., Guigue, A., Chabaud, M.A., Reeb, P.D., Mitra, A., Grau, Y., Soustelle, L., and Marion-Poll, F. (2015). Dual mechanism for bitter avoidance in Drosophila. J. Neurosci. *35*, 3990–4004.

Ganguly, A., Pang, L., Duong, V.K., Lee, A., Schoniger, H., Varady, E., and Dahanukar, A. (2017). A molecular and cellular context-dependent role for Ir76b in detection of amino acid taste. Cell Rep. *18*, 737–750.

Gendre, N., Lüer, K., Friche, S., Grillenzoni, N., Ramaekers, A., Technau, G.M., and Stocker, R.F. (2004). Integration of complex larval chemosensory organs into the adult nervous system of Drosophila. Development *131*, 83–92.

Hussain, A., Zhang, M., Üçpunar, H.K., Svensson, T., Quillery, E., Gompel, N., Ignell, R., and Grunwald Kadow, I.C. (2016). Ionotropic chemosensory receptors mediate the taste and smell of polyamines. PLoS Biol. *14*, e1002454.

Jeong, Y.T., Shim, J., Oh, S.R., Yoon, H.I., Kim, C.H., Moon, S.J., and Montell, C. (2013). An odorant-binding protein required for suppression of sweet taste by bitter chemicals. Neuron *79*, 725–737.

Joseph, R.M., and Heberlein, U. (2012). Tissue-specific activation of a single gustatory receptor produces opposing behavioral responses in Drosophila. Genetics *192*, 521–532.

Joseph, R.M., Sun, J.S., Tam, E., and Carlson, J.R. (2017). A receptor and neuron that activate a circuit limiting sucrose consumption. eLife *6*, e24992.

Kang, K., Pulver, S.R., Panzano, V.C., Chang, E.C., Griffith, L.C., Theobald, D.L., and Garrity, P.A. (2010). Analysis of Drosophila TRPA1 reveals an ancient origin for human chemical nociception. Nature *464*, 597–600.

Keene, A.C., and Masek, P. (2012). Optogenetic induction of aversive taste memory. Neuroscience *222*, 173–180.

Kim, H., Jeong, Y.T., Choi, M.S., Choi, J., Moon, S.J., and Kwon, J.Y. (2017). Involvement of a Gr2a-expressing Drosophila pharyngeal gustatory receptor neuron in regulation of aversion to high-salt foods. Mol Cells *40*, 331–338.

Koh, T.W., He, Z., Gorur-Shandilya, S., Menuz, K., Larter, N.K., Stewart, S., and Carlson, J.R. (2014). The Drosophila IR20a clade of ionotropic receptors are candidate taste and pheromone receptors. Neuron *83*, 850–865.

Kwon, J.Y., Dahanukar, A., Weiss, L.A., and Carlson, J.R. (2014). A map of taste neuron projections in the Drosophila CNS. J. Biosci. *39*, 565–574.

LeDue, E.E., Chen, Y.C., Jung, A.Y., Dahanukar, A., and Gordon, M.D. (2015). Pharyngeal sense organs drive robust sugar consumption in Drosophila. Nat. Commun. *6*, 6667.

Liman, E.R., Zhang, Y.V., and Montell, C. (2014). Peripheral coding of taste. Neuron *81*, 984–1000.

Ling, F., Dahanukar, A., Weiss, L.A., Kwon, J.Y., and Carlson, J.R. (2014). The molecular and cellular basis of taste coding in the legs of Drosophila. J. Neurosci. *34*, 7148–7164.

Marella, S., Fischler, W., Kong, P., Asgarian, S., Rueckert, E., and Scott, K. (2006). Imaging taste responses in the fly brain reveals a functional map of taste category and behavior. Neuron *49*, 285–295.

Miyamoto, T., and Amrein, H. (2014). Diverse roles for the Drosophila fructose sensor Gr43a. Fly (Austin) *8*, 19–25.

Miyamoto, T., Slone, J., Song, X., and Amrein, H. (2012). A fructose receptor functions as a nutrient sensor in the Drosophila brain. Cell *151*, 1113–1125.

Nayak, S.V., and Singh, R.N. (1983). Sensilla on the tarsal segments and mouthparts of adult Drosophila-melanogaster Meigen (Diptera, Drosophilidae). Int. J. Insect Morphol. Embryol. *12*, 273–291.

Ni, L., Klein, M., Svec, K.V., Budelli, G., Chang, E.C., Ferrer, A.J., Benton, R., Samuel, A.D., and Garrity, P.A. (2016). The ionotropic receptors IR21a and IR25a mediate cool sensing in Drosophila. eLife *5*, e13254.

Nottebohm, E., Dambly-Chaudière, C., and Ghysen, A. (1992). Connectivity of chemosensory neurons is controlled by the gene poxn in Drosophila. Nature *359*, 829–832.

Shim, J., Lee, Y., Jeong, Y.T., Kim, Y., Lee, M.G., Montell, C., and Moon, S.J. (2015). The full repertoire of Drosophila gustatory receptors for detecting an aversive compound. Nat. Commun. *6*, 8867.

Soldano, A., Alpizar, Y.A., Boonen, B., Franco, L., López-Requena, A., Liu, G., Mora, N., Yaksi, E., Voets, T., Vennekens, R., et al. (2016). Gustatory-mediated avoidance of bacterial lipopolysaccharides via TRPA1 activation in Drosophila. eLife *5*, e13133.

Stocker, R.F., and Schorderet, M. (1981). Cobalt filling of sensory projections from internal and external mouthparts in Drosophila. Cell Tissue Res. *216*, 513–523.

Thistle, R., Cameron, P., Ghorayshi, A., Dennison, L., and Scott, K. (2012). Contact chemoreceptors mediate male-male repulsion and male-female attraction during Drosophila courtship. Cell *149*, 1140–1151.

van Giesen, L., Hernandez-Nunez, L., Delasoie-Baranek, S., Colombo, M., Renaud, P., Bruggmann, R., Benton, R., Samuel, A.D., and Sprecher, S.G. (2016). Multimodal stimulus coding by a gustatory sensory neuron in Drosophila larvae. Nat. Commun. *7*, 10687.

Weiss, L.A., Dahanukar, A., Kwon, J.Y., Banerjee, D., and Carlson, J.R. (2011). The molecular and cellular basis of bitter taste in Drosophila. Neuron *69*, 258–272.

Yapici, N., Cohn, R., Schusterreiter, C., Ruta, V., and Vosshall, L.B. (2016). A taste circuit that regulates ingestion by integrating food and hunger signals. Cell *165*, 715–729.

Zhang, Y.V., Ni, J., and Montell, C. (2013). The molecular basis for attractive salt-taste coding in Drosophila. Science *340*, 1334–1338.